Vlasov code simulation of contact discontinuities

Cite as: Phys. Plasmas **26**, 102107 (2019); https://doi.org/10.1063/1.5100314
Submitted: 17 April 2019 . Accepted: 18 September 2019 . Published Online: 10 October 2019

Takayuki Umeda, Naru Tsujine, and Yasuhiro Nariyuki

Physics of Plasmas ARTICLE scitation.org/journal/php

Vlasov code simulation of contact discontinuities

Cite as: Phys. Plasmas **26**, 102107 (2019); doi: 10.1063/1.5100314
Submitted: 17 April 2019 · Accepted: 18 September 2019 ·
Published Online: 10 October 2019

Takayuki Umeda,[1,a)] Naru Tsujine,[2] and Yasuhiro Nariyuki[3,b)]

AFFILIATIONS

[1]Institute for Space-Earth Environmental Research, Nagoya University, Nagoya 464-8601, Japan
[2]Graduate School of Science and Engineering for Education, University of Toyama, Toyama 930-8555, Japan
[3]Faculty of Human Development, University of Toyama, Toyama 930-8555, Japan

[a)]Email: umeda@isee.nagoya-u.ac.jp
[b)]Email: nariyuki@edu.u-toyama.ac.jp

ABSTRACT

The stability of contact discontinuities formed by the relaxation of two Maxwellian plasmas with different number densities but the same plasma thermal pressure is studied by means of a one-dimensional electrostatic full Vlasov simulation. Our simulation runs with various combinations of ion-to-electron ratios of the high-density and low-density regions showed that transition layers of density and temperature without jump in the plasma thermal pressure are obtained when the electron temperatures in the high-density and low-density regions are almost equal to each other. However, the stable structure of the contact discontinuity with a sharp transition layer on the Debye scale is not maintained. It is suggested that non-Maxwellian velocity distributions are necessary for the stable structure of contact discontinuities.

I. INTRODUCTION

Contact discontinuity is one of the magneto-hydro-dynamic (MHD) discontinuities in a collisionless plasma. The contact discontinuity is characterized by a jump in both the plasma density and temperature across the discontinuity, while there is no jump in the flow velocity, the plasma thermal pressure and the magnetic field across the discontinuity. The normal flow velocity is zero in the rest frame of the discontinuity. A contact discontinuity in a collisionless kinetic plasma has never been demonstrated or simulated before Wu *et al.*,[1] although its existence is known in MHD[2] and Hall-MHD[3] simulations.

Wu *et al.*,[1] examined the stability of a contact discontinuity by means of a hybrid particle-in-cell (PIC) simulation, in which ions are treated as macroparticles, while electrons are treated as a massless fluid. They showed that the stable structure of the contact discontinuity was maintained by an electric field due to the gradient of the electron thermal pressure. Lapenta and Brackbill[4] also examined the stability of a contact discontinuity by means of a full PIC simulation, in which both ions and electrons are treated as macroparticles. They showed that the thickness of the contact discontinuity increased from its initial value in the ion time scale. The electric field in the full PIC simulation due to the charge separation at the discontinuity was not able to maintain the structure of the contact discontinuity, in contrast with the hybrid PIC simulation. It is noted that the initial electron-to-ion temperature ratio at both sides of the discontinuity was equal to each other ($T_{e1}/T_{i1} = T_{e2}/T_{i2}$) in these two past studies.[1,4] Here, the subscripts "1" and "2" denote the asymptotic quantities on the low-density and high-density sides of the discontinuity, respectively.

Later, Tsai *et al.*[5] proposed a temperature condition for contact discontinuities,

$$(T_{i1} - T_{i2})(T_{e1} - T_{e2}) < 0. \quad (1)$$

In the present study, we refer to this condition as the "Tsai condition." They also examined the stability of a contact discontinuity by means of a full Vlasov simulation, in which both ions and electrons are treated as velocity distribution functions. They allowed different initial ion-to-electron temperature ratios between the low-density and high-density sides of the discontinuity, i.e., $T_{e1}/T_{i1} \neq T_{e2}/T_{i2}$, but kept the continuity of the plasma thermal pressure, i.e., $N_1(T_{i1} + T_{e1}) = N_2(T_{i2} + T_{e2})$. Here, the ion density and the electron density are almost equal to each other due to the MHD regime. They suggested that the stable structure of the transition layers of density and temperature without jump in the plasma thermal pressure (i.e., $P_{i1} + P_{e1} = P_{i2} + P_{e2}$) was maintained "in the electron time scale," when the discontinuity satisfied the Tsai condition. In the present study, we refer to this transition layer as the "Tsai transition layer." Tsai *et al.*[5] also argued that the parameter used in the previous full PIC simulation study[4] did not satisfy the Tsai condition.

Hsieh *et al.*[6] showed evidence of contact discontinuities in natural plasma based on the *in situ* observation by the THEMIS spacecraft. They suggested that the parameter of the observed contact

discontinuities satisfied the Tsai condition. The thickness of the transition layer of the observed contact discontinuities was estimated as $\delta/r_i \approx 4 \sim 12$, where r_i represents the ion gyroradius. Based on the plasma beta (i.e., the ratio of the plasma thermal pressure to the magnetic pressure) of $\beta \approx 0.18$, the thickness of the transition layer of the observed contact discontinuities is re-estimated as several tens of the ion Debye length.

We re-examine the stability of contact discontinuities by means of a full Vlasov simulation. The purpose of the present study is two-fold. First, we use parameters close to the observed ones, since the density and temperature ratios used in the past simulation studies[1,4,5] (e.g., $N_1/N_2 = 1/4, 1/3$, $T_{e2}/T_{i2} = 5$) were different from the observed ones ($N_1/N_2 \approx 2/3$, $T_{e2}/T_{i2} \approx 0.3$).[6] Second, we study a long-time evolution of the transition layer of discontinuities in the ion time scale, since the previous study[5] showed its time evolution in the electron time scale up to $1000/\omega_{pe}$.

II. SIMULATION SETUP

We use a one-dimensional (1D) electrostatic Vlasov code based on the splitting scheme[7] with the fifth-order version of the positivity-preserving, nonoscillatory and conservative scheme.[8,9] The velocity distribution functions for ions and electrons are defined in the $x - v_x$ phase space, and are updated by the Vlasov equation

$$\frac{\partial}{\partial t} f_s[t,x,v_x] + v_x \frac{\partial}{\partial x} f_s[t,x,v_x] + \frac{q_s}{m_s} E_x[t,x] \frac{\partial}{\partial v_x} f_s[t,x,v_x] = 0, \quad (2)$$

where the subscript s represents particles species (with $s = i$ and e being the ions and electrons, respectively). In the one-dimensional electrostatic limit, the effects of the magnetic field are neglected when the magnetic field is taken in the x direction. The electrostatic field E_x is given by solving the Poisson equation,

$$\frac{\partial}{\partial x} E_x[t,x] = \frac{\rho[t,x]}{\epsilon_0} = \frac{1}{\epsilon_0} \sum_s q_s \int f_s[t,x,v_x] \mathrm{d}v_x. \quad (3)$$

We impose continuous boundary conditions ($\partial/\partial x = 0$) for the velocity distribution functions, with which an open boundary condition for acoustic modes is realized.

The present simulation model is identical to the past simulation studies.[1,4,5] We study the stability of the transition region between two Maxwellian plasmas with different densities and temperatures but the same plasma thermal pressure. The spatial profiles of the initial number density for ions and electrons are given by

$$N_i[x] = N_e[x] = N_0[x] = \frac{N_1 + N_2}{2} - \frac{N_1 - N_2}{2} \tanh\left[\frac{x}{\delta_0}\right], \quad (4)$$

where δ_0 represents the initial half thickness of the transition layer. The spatial profiles of the initial temperature for ions and electrons are given by

$$T_{i0}[x] = \frac{2P_0 T_{i1} T_{i2}}{N_0[x]\left\{2T_{i1}T_{i2} + T_{i1}T_{e2} + T_{i2}T_{e1} + (T_{i1}T_{e2} - T_{i2}T_{e1})\tanh\left[\frac{x}{\delta_0}\right]\right\}}, \quad (5)$$

$$T_{e0}[x] = \frac{P_0\left\{T_{i1}T_{e2} + T_{i2}T_{e1} + (T_{i1}T_{e2} - T_{i2}T_{e1})\tanh\left[\frac{x}{\delta_0}\right]\right\}}{N_0[x]\left\{2T_{i1}T_{i2} + T_{i1}T_{e2} + T_{i2}T_{e1} + (T_{i1}T_{e2} - T_{i2}T_{e1})\tanh\left[\frac{x}{\delta_0}\right]\right\}}, \quad (6)$$

where $P_0 \equiv (T_{i1} + T_{e1})N_1 = (T_{i2} + T_{e2})N_2$ is the initial plasma thermal pressure. With these spatial profiles of the temperature, the initial spatial profile of the electron-to-ion temperature ratio $T_{e0}[x]/T_{i0}[x]$ has a form of the "tanh" function. The initial velocity distribution functions for ions and electrons are given by

$$f_{0s}[x,v_x] = N_0[x]\sqrt{\frac{m_s}{2\pi T_{s0}[x]}} \exp\left[-\frac{m_s v_x^2}{2T_{s0}[x]}\right]. \quad (7)$$

We performed nine different simulation runs with several combination of T_{e1}/T_{i1}, T_{e2}/T_{i2}, and N_1/N_2. The parameters of the present study are shown in Table I. The parameters in run C correspond to "Event 2" of the THEMIS observation in Ref. 6. In runs A–F, we vary T_{e1}/T_{i1} by fixing T_{e2}/T_{i2} and N_1/N_2 based on the *in situ* observation.[6] In runs G–I, we vary T_{e1}/T_{i1} by fixing T_{e2}/T_{i2} and N_1/N_2 based on the past simulation studies.[1,4,5]

Figure 1 shows these parameters in T_{e1}/T_{i1} vs T_{e2}/T_{i2} space with $N_1/N_2 = 2.08/2.86$ and $N_1/N_2 = 1/3$ for panels (a) and (b),

TABLE I. Parameters of different simulation runs for the present study. The potential jump across the transition layer, $\Delta\phi = \phi_2 - \phi_1$, is normalized by eT_{e2}/m_e.

Run	T_{e1}/T_{i1}	T_{e2}/T_{i2}	N_1/N_2	Tsai condition[5]	T_{e1}/T_{e2}	$\Delta\phi$
A	0.0536	0.304	0.727	Negative	0.3	1.8
B	0.1569	0.304	0.727	Negative	0.8	1.0
C	0.2000	0.304	0.727	Negative	0.983	0.7
D	0.2554	0.304	0.727	Positive	1.2	0.3
E	0.4050	0.304	0.727	Positive	1.7	−0.6
F	0.8443	0.304	0.727	Negative	2.7	−2.6
G	0.1250	5	0.333	Negative	0.4	3.2
H	0.5000	5	0.333	Positive	1.2	1.9
I	17.947	5	0.333	Negative	3.41	−1.7

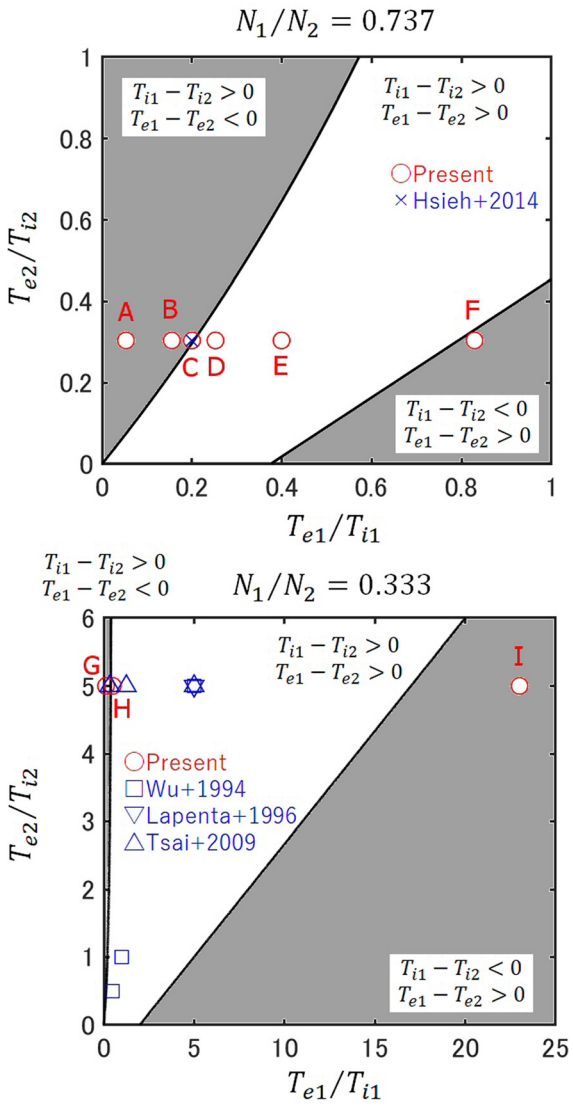

FIG. 1. Parameters of different simulation runs for the present study in the T_{e1}/T_{i1} vs T_{e2}/T_{i2} space. (a)$N_1/N_2 = 0.737$. (b)$N_1/N_2 = 0.333$. The parameters of the past studies[1,4–6] are also superimposed.

respectively. The parameters of the past studies[1,4–6] are also superimposed. The solid curves show the boundary of the Tsai condition, which depends on N_1/N_2. The left curve and the right curve correspond to $T_{e1} = T_{e2}$ and $T_{i1} = T_{i2}$, respectively. The gray regions satisfy the Tsai condition, while the white region at the center does not satisfy the Tsai condition due to $T_{i1} - T_{i2} > 0$ and $T_{e1} - T_{e2} > 0$. It is seen that the parameters of the past two studies[1,4] did not satisfy the Tsai condition. (Note that $N_1/N_2 = 1/4$ in these past two studies.) One of three parameters (case 2: $T_{e1}/T_{i1} = 0.33$) in Ref. 5 satisfied the Tsai condition. The parameters of the *in situ* observation[6] also satisfied the Tsai condition. In the present study, the Tsai condition is satisfied in runs A, B, C, F, G, and I.

The parameters are normalized with respect to the electron plasma frequency and the thermal velocity in the high-density region, i.e., $\omega_{pe2} \equiv \sqrt{q_e^2 N_2/(\epsilon_0 m_e)}$ and $V_{te2} \equiv \sqrt{T_{e2}/m_e}$. Note that the normalization of the present study is different from that of Tsai *et al.*[5] where the parameters are normalized with respect to the electron quantities in the low-density region. The number of grids for the configuration space and the velocity space is $N_x = 12\,000$ and $N_{vx} = 1000$, respectively. The grid spacing for the configuration space and the velocity space is $\Delta x = 0.5\lambda_{De2} \equiv 0.5V_{te2}/\omega_{pe2}$, $\Delta v_{xe} = 0.032V_{te2}$, and $\Delta v_{xi} = 0.0016V_{te2}$. The time step is set as $\Delta t = 0.025/\omega_{pe2}$. The real ion-to-electron mass ratio $m_i/m_e = 1836$ is used. The initial half-thickness of the transition layer is set as $\delta_0 = 2\lambda_{De2}$. It should be noted, however, that the initial thickness does not affect our conclusion.

III. RESULT

Figures 2 and 3 show the spatial profiles of the ion and electron densities, N_i and N_e, the ion and electron temperatures, T_i and T_e, the ion and electron thermal pressures, P_i and P_e, the total plasma thermal pressure $P = P_i + P_e$, the electric potential ϕ, and $x - v_x$ phase space of electrons at $\omega_{pe2}t = 1000$ and 10 000 in runs A–F. The spatial profiles of N_i, N_e, T_i, T_e, P_i, P_e, P, and ϕ at $\omega_{pe2}t = 100$ are also shown by the dashed lines as references. In all of the simulation runs, the transition layer of the ion pressure continues to evolve at $\omega_{pe2}t = 10\,000$, suggesting that the transition layer is not in the steady state. We have confirmed that the quasi charge neutrality $N_i \approx N_e$ is almost satisfied in all of the simulation runs as shown in Figs. 2 and 3. An electric potential is generated in the transition layer due to the charge separation in the spatial scale of the Debye length. At $\omega_{pe2}t = 1000$ (in the electron scale), the electron phase-space distributions evolve in association with the electron motion across the transition layer. At $\omega_{pe2}t = 10\,000$ (in the ion time scale), by contrast, the electron phase-space distributions are modified in association with the ion motion across the transition layer.

In run A, the electron pressure in the low-density region ($x < 0$) increases from its initial value, while the electron pressure in the high-density region ($x > 0$) decreases from its initial value. Electron phase-space holes and ion acoustic waves are also excited due to electron acceleration by the electric potential at the transition layer (see Figs. 2 and 3), which is similar to the wave generation processes at double layers.[10] The electron pressure P_e is enhanced locally by these waves in run A. In runs E and F, on the other hand, the electron pressure in the low-density region decreases from its initial value, while the electron pressure in the high-density region increases from its initial value.

In run B, the electron pressure in the low-density region increases slightly from its initial value, while the electron pressure in the high-density region decreases slightly from its initial value. In run C, the electron pressure is almost the same as its initial value. In run D, the electron pressure in the low-density region decreases slightly from its initial value, while the electron pressure in the high-density region increases slightly from its initial value. The continuity of the plasma thermal pressure ($P_i + P_e =$ const.) across the transition layer is almost satisfied (the Tsai transition layer) in these three runs where the initial electrons pressure satisfies $P_{e1}/P_{e2} \approx 1$.

In Table I, we show T_{e1}/T_{e2} in different simulation runs,

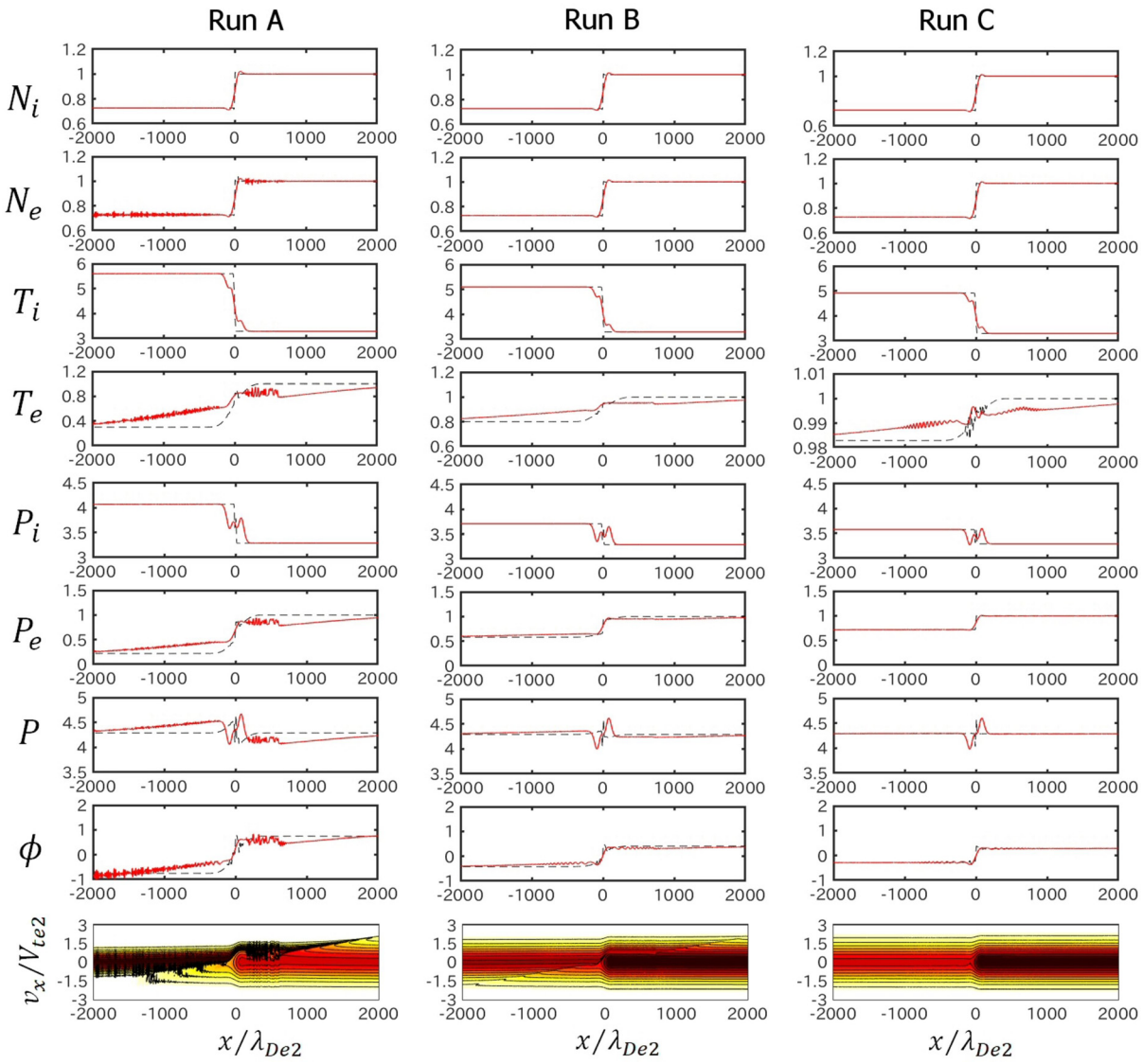

FIG. 2. Spatial profiles of the ion and electron densities, N_i and N_e, the ion and electron temperatures, T_i and T_e, the ion and electron thermal pressures, P_i and P_e, the total plasma thermal pressure $P = P_i + P_e$, the electric potential ϕ, and $x - v_x$ phase space of electrons at $\omega_{pe2}t = 1000$ (solid lines) in runs A–F. The density, temperature, pressure, and potential are normalized by N_{e2}, T_{e2}, P_{e2}, and eT_{e2}/m_e, respectively. The spatial profiles of N_i, N_e, T_i, T_e, P_i, P_e, P, and ϕ at $\omega_{pe2}t = 100$ are also shown by the dashed lines as references.

$$\frac{T_{e1}}{T_{e2}} = \frac{N_2}{N_1}\frac{1+\frac{T_{i2}}{T_{e2}}}{1+\frac{T_{i1}}{T_{e1}}}, \tag{8}$$

which is derived from $N_1(T_{e1} + T_{i1}) = N_2(T_{e2} + T_{i2})$. Although the Tsai condition[5] is satisfied in runs A and F, the Tsai transition layers are not obtained. On the other hand, the Tsai transition layer is obtained in run D, although the Tsai condition[5] is not satisfied. The present simulation results indicate that the Tsai transition layers are not obtained by the Tsai condition,[5] but are obtained by $T_{e1} \approx T_{e2}$.

Tsai *et al.*[5] performed simulation runs with $T_{e2}/T_{i2} = 5$ and $N_1/N_2 = 1/3$. The continuity of the plasma thermal pressure ($P_i + P_e \approx$ const.) across the transition layer (i.e., the Tsai transition layer) was obtained in case 2 ($T_{e1}/T_{e2} = 0.8932$) of Ref. 5. Although the parameter $T_{e1}/T_{e2} = 0.8932$ in case 2 of Ref. 5 satisfied the Tsai condition, this parameter also satisfied $T_{e1} \approx T_{e2}$. To confirm the indication that the Tsai transition layers are obtained with $T_{e1} \approx T_{e2}$, we performed additional three simulation runs G–I with the same parameter ($T_{e2}/T_{i2} = 5$ and $N_1/N_2 = 1/3$) as Ref. 5 but with different T_{e1}/T_{e2}.

Figures 4 and 5 show the spatial profiles of the ion and electron densities, N_i and N_e, the ion and electron temperatures, T_i and T_e, the ion and electron thermal pressures, P_i and P_e, the total plasma thermal pressure $P = P_i + P_e$, the electric potential ϕ, and $x - v_x$ phase space of electrons at $\omega_{pe2}t = 1000$ and 10 000 in runs G–I. The spatial

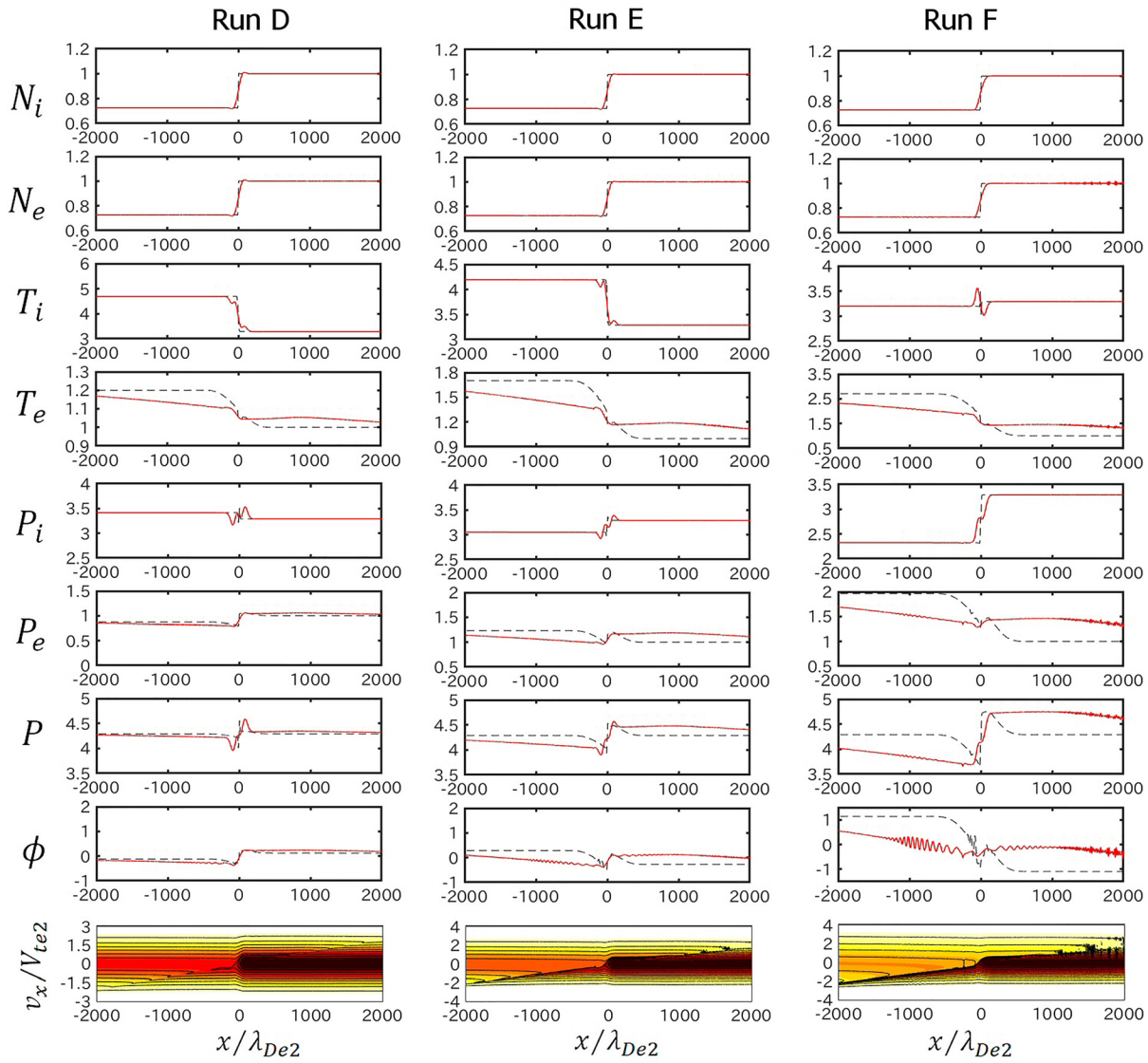

FIG. 2. (*Continued*).

profiles of N_i, N_e, T_i, T_e, P_i, P_e, P, and ϕ at $\omega_{pe2}t = 100$ are also shown by the dashed lines as references. In run G, the electron pressure in the low-density region increases from its initial value, while the electron pressure in the high-density region decreases from its initial value. Electron phase-space holes and ion acoustic waves are also excited as in run A. In run H, the electron pressure in the low-density region decreases slightly from its initial value, while the electron pressure in the high-density region increases slightly from its initial value. In run I, the electron pressure in the low-density region decreases from its initial value, while the electron pressure in the high-density region increases from its initial value. The results of runs G–I are consistent with those of runs A–F. The Tsai transition layer is obtained in run H, in which the temperature ratio is $T_{e1} \approx T_{e2}$ but the Tsai condition[5] is not satisfied. In runs G and I, on the other hand, the Tsai transition layers are not obtained although the Tsai condition[5] is satisfied. Hence, it is also confirmed in the runs with $T_{e2}/T_{i2} = 5$ and $N_1/N_2 = 1/3$ that the Tsai transition layers are not obtained by the Tsai condition,[5] but are obtained by $T_{e1} \approx T_{e2}$.

In Table I, we show the potential jump across the transition layer, $\Delta\phi \equiv \phi_2 - \phi_1$, averaged for $\omega_{pe2}t = 250 \sim 500$. Here, the values of the potential at $x/\lambda_{De2} = -3000$ and $x/\lambda_{De2} = 3000$ are adopted as ϕ_1 and ϕ_2, respectively. Note that we use an averaged value of the potential jump because ϕ_1 and ϕ_2 oscillate at a period of $T \approx 250\omega_{pe2} \approx 2\pi/\omega_{pi2}$. The potential is normalized by eT_{e2}/m_e.

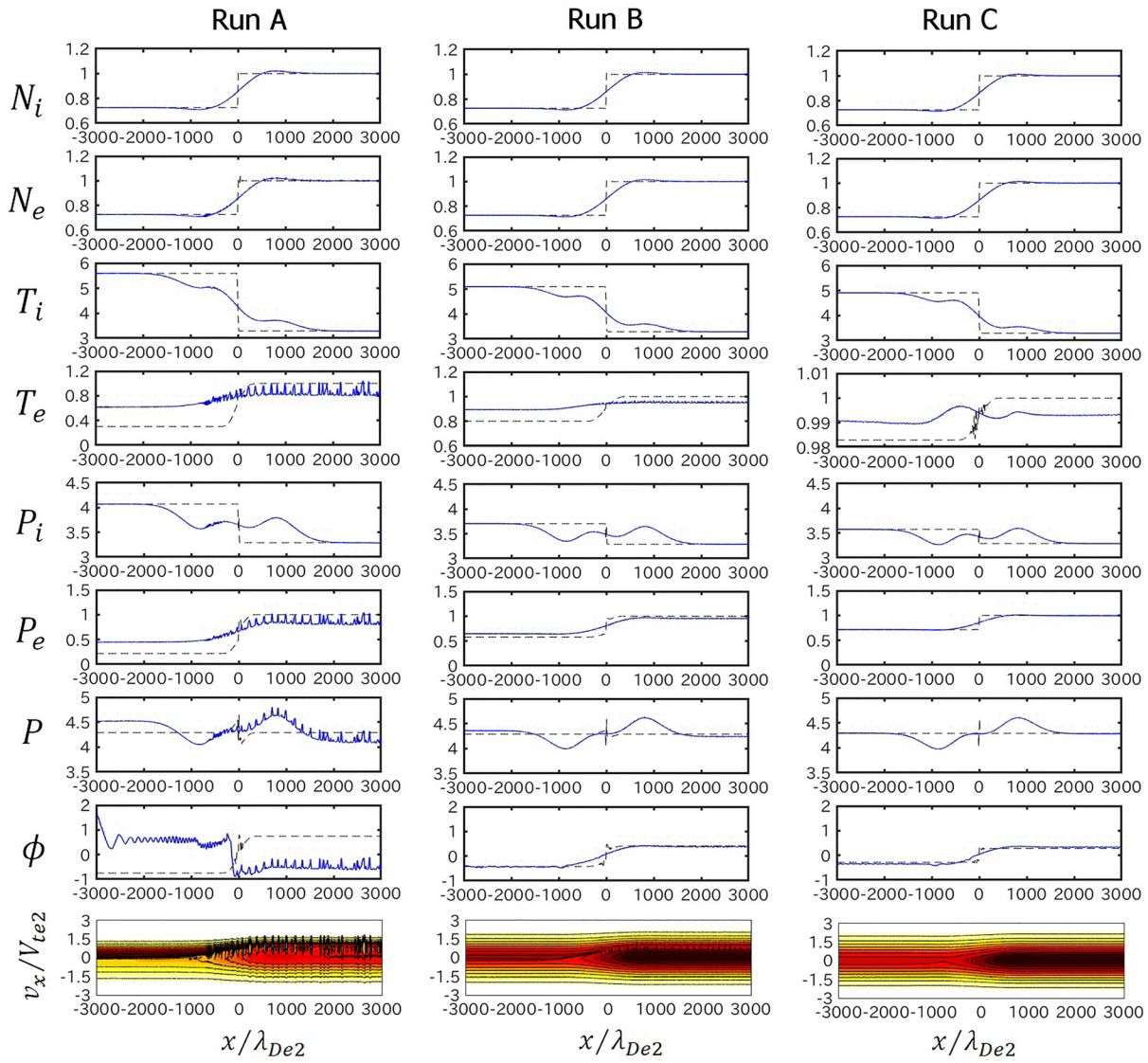

FIG. 3. Spatial profiles of the ion and electron densities, N_i and N_e, the ion and electron temperatures, T_i and T_e, the ion and electron thermal pressures, P_i and P_e, the total plasma thermal pressure $P = P_i + P_e$, the electric potential ϕ, and $x - v_x$ phase space of electrons at $\omega_{pe2}t = 10\,000$ in runs A–F with the same format as Fig. 2.

We found that there is a positive correlation between $\Delta\phi$ and $T_{e2} - T_{e1}N_1/N_2$. This result suggests that the electric potential is associated with the jump in the initial electron pressure.

To study the stability of the Tsai transition layer in run C, we estimate the half-thickness of the transition layer of the ion density by fitting the tanh function. The solid line in Fig. 6 shows the half-thickness of the ion transition layer δ_{N_i} as a function of time. The thickness increases linearly in time from its initial value ($\delta_{N_i} = 2\lambda_{De2}$). We performed another simulation run "without" the electric field but with the same initial parameters as run C. In this run, the two ion components from the two sides mix across the transition layer by the free streaming. The ion density profile relaxes with the thickness of the density transition region linearly proportional to time.[1] The half-thickness of the ion transition layer as a function of time in this run is shown by the dashed line. It is clearly seen that there is no difference between the two lines. This means that a stable structure of the contact discontinuity with the thickness of several tens of the ion Debye length is not obtained in run C, although the parameters of the *in situ* observation[6] are used.

We also checked the half-thickness of the ion transition layer in other runs (but not shown here). We confirmed that the half-thickness increases linearly as the free streaming at the ion thermal velocity in all of the simulation runs. The present simulation study suggests that the electric potential due to the charge separation at the transition layer of the discontinuity is too small to disturb ion motion across the

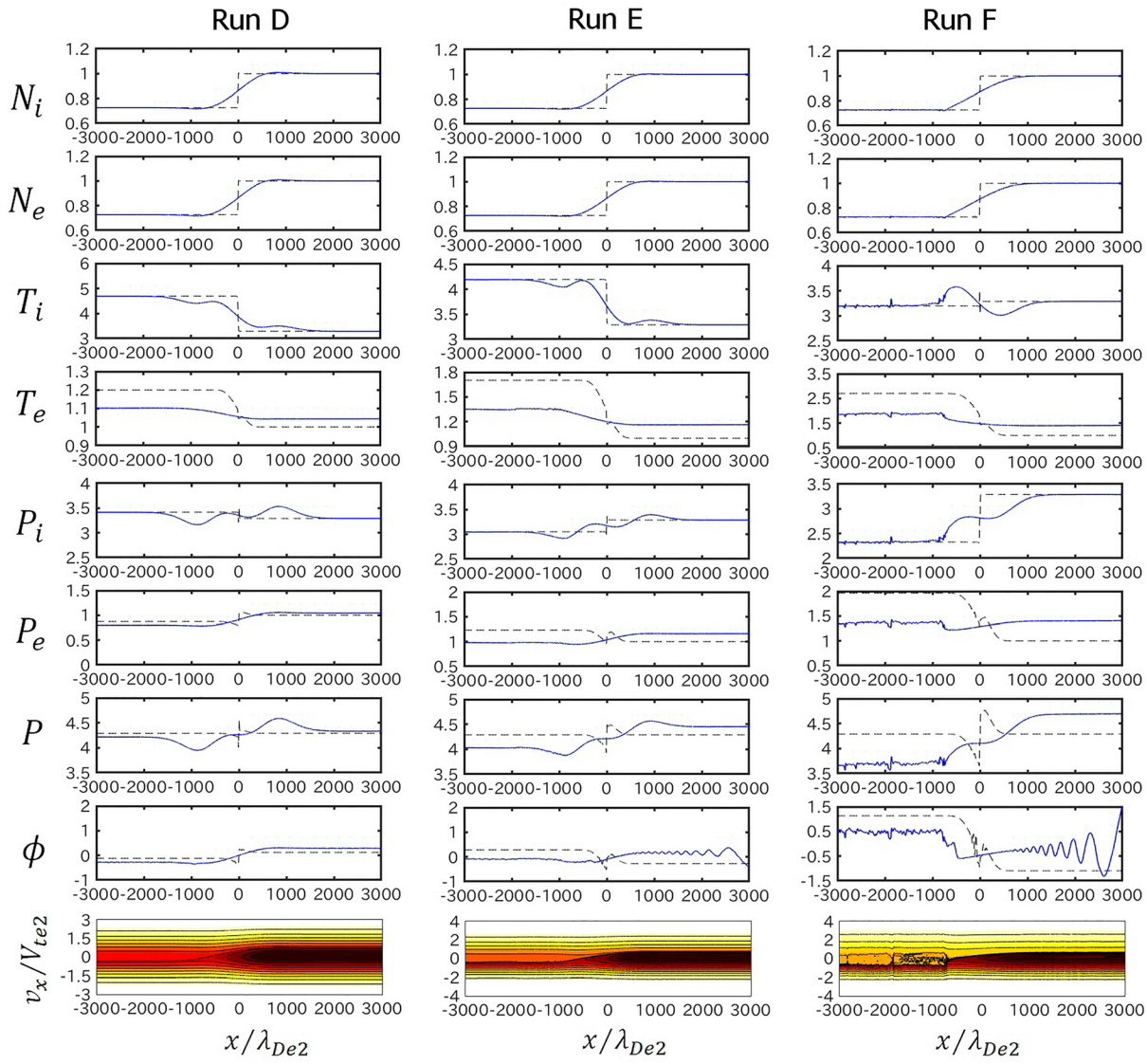

FIG. 3. (*Continued*).

transition layer. The structure of transition layers in the present study is not maintained even in the electron time scale, which is consistent with the previous study.[4]

IV. DISCUSSION

A velocity distribution function in the Vlasov-Poisson equilibrium is expressed by a function of the Hamiltonian.[11] Suppose that an equilibrium solution of the velocity distribution function is expressed by

$$f_s[x, v_x] = N_{s0}\sqrt{\frac{m_s}{2\pi T_s}}\exp\left[-\frac{m_s v_x^2}{2T_s} - \frac{q_s\phi[x]}{T_s}\right]. \tag{9}$$

Inserting this velocity distribution function into the time-independent Vlasov equation, one can easily obtain

$$v_x\frac{\partial N_{s0}}{\partial x} - \frac{q_s}{m_s}\frac{\partial\phi}{\partial x}\frac{\partial N_{s0}}{\partial v_x} = 0 \tag{10}$$

and

$$v_x\frac{\partial T_s}{\partial x} - \frac{q_s}{m_s}\frac{\partial\phi}{\partial x}\frac{\partial T_s}{\partial v_x} = 0. \tag{11}$$

A Maxwellian velocity distribution function with $\partial N_{s0}/\partial v_x = 0$ and $\partial T_s/\partial v_x = 0$ gives an equilibrium solution as $\partial N_{s0}/\partial x = \partial T_s/\partial x = 0$. Hence, the simple Maxwellian velocity distribution

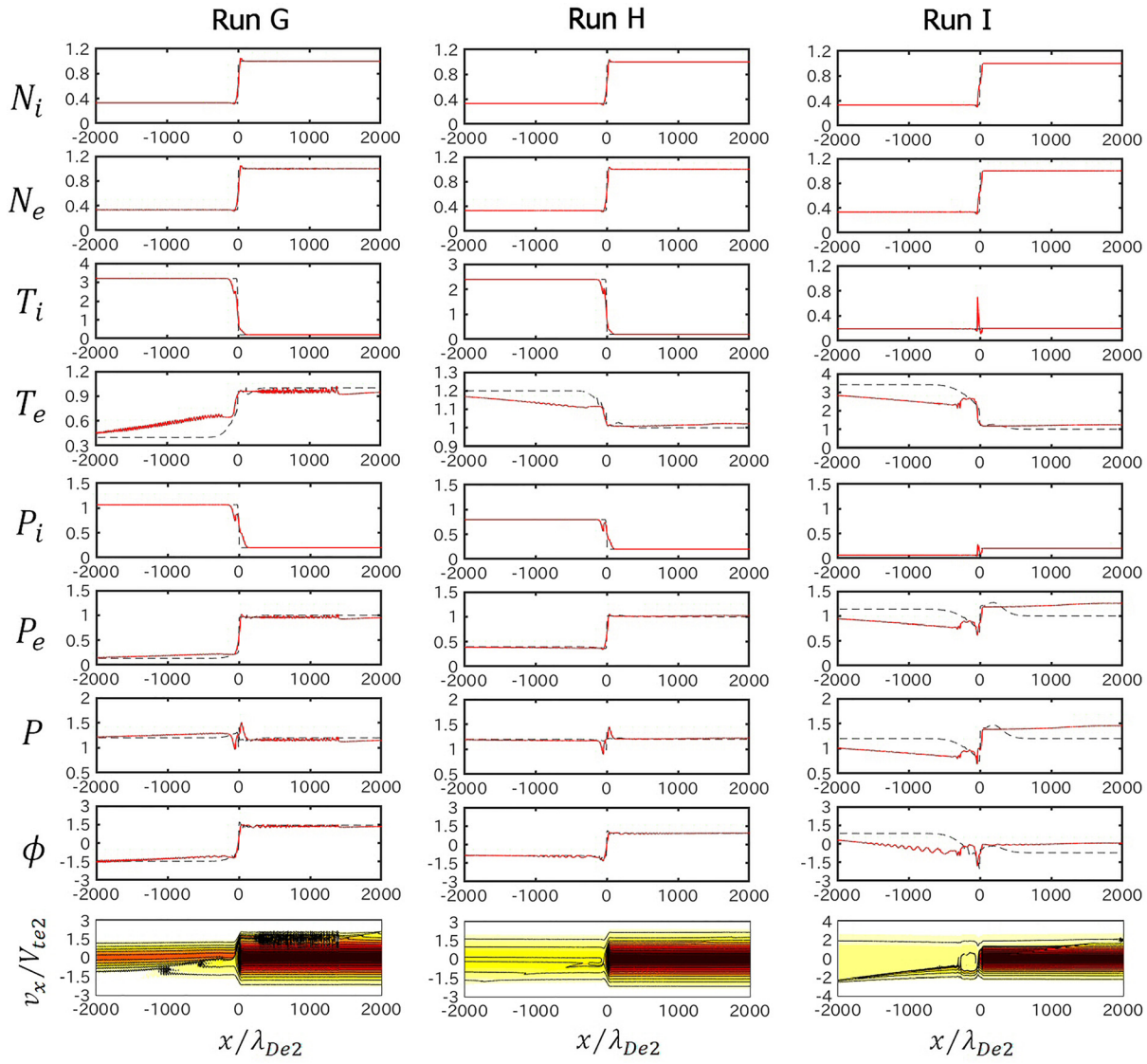

FIG. 4. Spatial profiles of the ion and electron densities, N_i and N_e, the ion and electron temperatures, T_i and T_e, the ion and electron thermal pressures, P_i and P_e, the total plasma thermal pressure $P = P_i + P_e$, the electric potential ϕ, and $x - v_x$ phase space of electrons at $\omega_{pe2}t = 1000$ (solid lines) in runs G–I with the same format as Fig. 2. The spatial profiles of N_i, N_e, T_i, T_e, P_i, P_e, P, and ϕ at $\omega_{pe2}t = 100$ are also shown by the dashed lines as references.

function with inhomogeneous temperature in Eq. (7) cannot be the Vlasov-Poisson equilibrium. Note that the condition $\partial T_s/\partial x = 0$ was missing in Tsai *et al.*[5]

Integration of the velocity distribution function (9) over the velocity gives the spatial profiles of the number density as

$$N_s[x] = \int_{-\infty}^{\infty} f_s[x, v_x]\mathrm{d}v_x = N_{s0} \exp\left[-\frac{q_s\phi[x]}{T_s}\right]. \quad (12)$$

This equation gives the boundary conditions of the density as $N_{i1} = N_{i0}\exp[-\frac{e\phi_1}{T_i}]$, $N_{e1} = N_{e0}\exp[\frac{e\phi_1}{T_e}]$, $N_{i2} = N_{i0}\exp[-\frac{e\phi_2}{T_i}]$, $N_{e2} = N_{e0}\exp[\frac{e\phi_2}{T_e}]$. We obtain the following equation from the quasi charge neutrality,

$$\frac{N_{i0}}{N_{e0}} = \exp\left[e\phi_1\left(\frac{1}{T_e}+\frac{1}{T_i}\right)\right] = \exp\left[e\phi_2\left(\frac{1}{T_e}+\frac{1}{T_i}\right)\right]. \quad (13)$$

This equation is satisfied only when $\phi_1 = \phi_2$. The Vlasov-Poisson equilibrium suggests that it is impossible to satisfy both $N_{e1} = N_{i1}$ and $N_{e2} = N_{i2}$ expect for $\phi_1 = \phi_2$. As shown by the present study, the potential gap across the transition layer is associated with the jump in the initial electron pressure. The Vlasov-Poisson equilibrium cannot be expressed by a simple Maxwellian-type velocity distribution function. Hence, the Tsai condition[5] based on the Vlasov theory with the Maxwellian velocity distribution functions is not satisfied.

Finally, the differences between the previous study[5] and the present study are summarized as follows. First, Tsai *et al.*[5] defined the

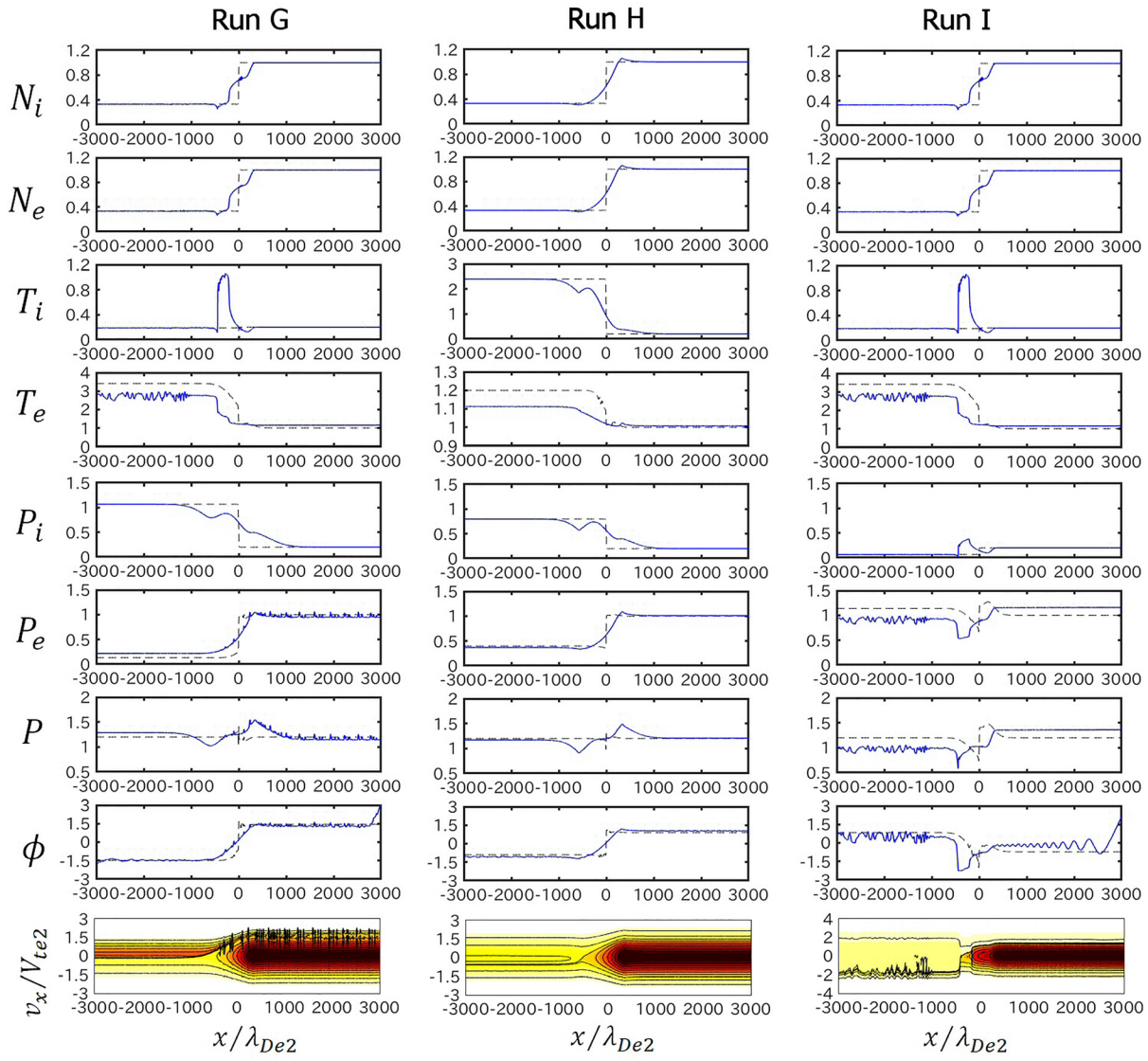

FIG. 5. Spatial profiles of the ion and electron densities, N_i and N_e, the ion and electron temperatures, T_i and T_e, the ion and electron thermal pressures, P_i and P_e, the total plasma thermal pressure $P = P_i + P_e$, the electric potential ϕ, and $x - v_x$ phase space of electrons at $\omega_{pe2}t = 10\,000$ in runs G–I with the same format as Fig. 4.

contact discontinuity as a transition layer of density and temperature without a jump in the plasma thermal pressure. They suggested that the structure was stable in the electron time scale. On the other hand, we have shown that the thickness of such a transition layer increases linearly in time on both electron and ion time scales, which is consistent with a previous study.[4] It is noted that the present and previous simulation studies cannot explain the THEMIS observation[6] in which a stable structure of the transition layer with a thickness of several tens of the ion Debye length was observed.

Second, Tsai *et al.*[5] chose the simulation parameters in a limited range of T_{e1}/T_{i1}. The parameter of case 2 in Ref. 5 incidentally satisfied both the Tsai condition and $T_{e1} \approx T_{i1}$. On the other hand, we have chosen the simulation parameters in a wide range of T_{e1}/T_{i1}. We

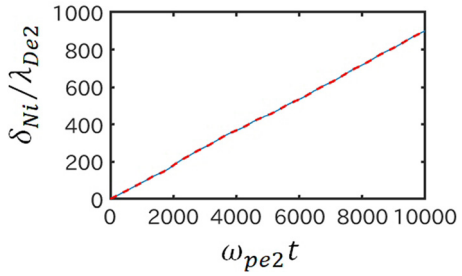

FIG. 6. Half-thickness of the ion transition layer δ_{N_i} as a function of time in run C. The half-thickness of the ion transition layer as a function of time in the run without the electric field is also shown by the dashed line.

have checked the validity of the Tsai condition and have obtained a correct condition for the formation of a transition layer of density and temperature without a jump in the plasma thermal pressure (i.e., the Tsai transition layer).

V. CONCLUSION

1. The structure of transition layers of density and temperature formed by the relaxation of two Maxwellian plasmas with different number densities but the same plasma thermal pressure (i.e., the Tsai transition layers) is not stable, which is consistent with the previous study.[4]
2. The Tsai transition layers are not obtained by the Tsai condition,[5] but are obtained by $T_{e1} \approx T_{e2}$.
3. Non-Maxwellian velocity distribution functions are necessary as a Vlasov-Poisson equilibrium for the stable structure of contact discontinuities, which is left as a future study.

ACKNOWLEDGMENTS

This work was supported by MEXT/JSPS Grant-In-Aid (KAKENHI) for Scientific Research (B) No. JP19H01868. This work was also carried out under the joint research program at the Institute for Space-Earth Environmental Research (ISEE) in Nagoya University. The computer simulations were performed on the CIDAS supercomputer system at ISEE, Nagoya University. We are grateful to Takayuki Haruki for the discussions.

REFERENCES

[1]B. Wu, H. J. K. Chao, W. H. Tsai, Y. Lin, and L. C. Lee, Geophys. Res. Lett. **21**, 2059–2062, https://doi.org/10.1029/94GL01579 (1994).
[2]M. Brio and C. C. Wu, J. Comput. Phys. **75**, 400–422 (1988).
[3]N. Omidi and D. Winske, J. Geophys. Res. **100**, 11935–11955, https://doi.org/10.1029/94JA02937 (1995).
[4]G. Lapenta and J. U. Brackbill, Geophys. Res. Lett. **23**, 1713–1716, https://doi.org/10.1029/96GL01845 (1996).
[5]T. C. Tsai, L. H. Lyu, J. K. Chao, M. Q. Chen, and W. H. Tsai, J. Geophys. Res. **114**, A12103, https://doi.org/10.1029/2009JA014121 (2009).
[6]W.-C. Hsieh, J.-H. Shue, J.-K. Chao, T.-C. Tsai, Z. Nemecek, and J. Safrankova, Geophys. Res. Lett. **41**, 8228–8234, https://doi.org/10.1002/2014GL062342 (2014).
[7]C. Z. Cheng and G. Knorr, J. Comput. Phys. **22**, 330–351 (1976).
[8]T. Umeda, Earth Planets Space **60**, 773–779 (2008).
[9]T. Umeda, Y. Nariyuki, and D. Kariya, Comput. Phys. Commun. **183**, 1094–1100 (2012).
[10]D. L. Newman, M. V. Goldman, R. E. Ergun, and A. Mangeney, Phys. Rev. Lett. **87**, 255001 (2001).
[11]I. B. Bernstein, J. M. Greene, and M. D. Kruskal, Phys. Rev. **108**, 546–550 (1957).